

Design and analysis of a flip-chip architecture for SAW-DQD strong coupling

Yi-Bo Wang(王奕博), Xiang-Xiang Song(宋骧骧), Zhuo-Zhi Zhang(张拙之), and Guo-Ping Guo(郭国平)
Citation: Chin. Phys. B, 2026, 35 (**2**): 024302. DOI: 10.1088/1674-1056/ae0895
http://cpb.iphy.ac.cn; http://iopscience.iop.org/cpb

What follows is a list of articles you may be interested in

Behaviors of cavitation bubbles driven by high-intensity ultrasound

Chen-Yang Huang(黄晨阳), Fan Li(李凡), Shi-Yi Feng(冯释毅), Cheng-Hui Wang(王成会), Shi Chen(陈时), Jing Hu(胡静), Xin-Rui He(何芯蕊), and Jia-Kai Song(宋家凯)
Chin. Phys. B, 2024, 33 (**2**): 024301. DOI: 10.1088/1674-1056/ad0717

Temperature-dependent subband mobility characteristics in n-doped silicon junctionless nanowire transistor

Ya-Mei Dou(窦亚梅), Wei-Hua Han(韩伟华), Yang-Yan Guo(郭仰岩), Xiao-Song Zhao(赵晓松), Xiao-Di Zhang(张晓迪), Xin-Yu Wu(吴歆宇), Fu-Hua Yang(杨富华)
Chin. Phys. B, 2019, 28 (**6**): 066804. DOI: 10.1088/1674-1056/28/6/066804

Investigation of a silicon-based one-dimensional phononic crystal plate via the super-cell plane wave expansion method

Zhu Xue-Feng(祝雪丰), Liu Sheng-Chun(刘盛春), Xu Tao(徐涛), Wang Tie-Hai(王铁海), and Cheng Jian-Chun(程建春)
Chin. Phys. B, 2010, 19 (**4**): 044301. DOI: 10.1088/1674-1056/19/4/044301

Design and analysis of a flip-chip architecture for SAW-DQD strong coupling

Yi-Bo Wang(王奕博)[1,2,3,4], Xiang-Xiang Song(宋骧骧)[1,2,3,4], Zhuo-Zhi Zhang(张拙之)[1,2,3,4,†], and Guo-Ping Guo(郭国平)[1,2,3,4,5]

[1] *Key Laboratory of Quantum Information, University of Science and Technology of China, Hefei* 230026, *China*
[2] *Suzhou Institute for Advanced Research, University of Science and Technology of China, Suzhou* 215123, *China*
[3] *CAS Center for Excellence in Quantum Information and Quantum Physics, University of Science and Technology of China, Hefei* 230026, *China*
[4] *Anhui Province Key Laboratory of Quantum Network, University of Science and Technology of China, Hefei* 230026, *China*
[5] *Origin Quantum Computing Company Limited, Hefei* 230088, *China*

(Received 14 July 2025; revised manuscript received 17 September 2025; accepted manuscript online 18 September 2025)

Surface acoustic wave (SAW) resonators offer distinct advantages for coupling to semiconductor qubits, including low loss, high stability, and compatibility with magnetic fields. However, the integration of SAW resonators with double quantum dots (DQDs) that host charge and spin qubits remains largely unexplored. In this work, we propose a flip-chip architecture that enables three-dimensional integration of a semiconductor DQD with a SAW resonator. Taking experimental feasibility into account, we estimate the coupling strength between a DQD and a SAW resonator. The results suggest that the strong coupling regime can be reached in our design. This study provides theoretical insight and practical guidance for experimental exploration of phonon–electron coupling in hybrid SAW-DQD quantum systems.

Keywords: surface acoustic wave resonator, double quantum dot, 3D integration, strong coupling

PACS: 43.35.Pt, 43.58.Kr, 68.65.Hb, 03.67.Lx

DOI: 10.1088/1674-1056/ae0895 **CSTR:** 32038.14.CPB.ae0895

1. Introduction

Surface acoustic waves (SAWs) are elastic waves that propagate along the surface of a solid. They are characterized[1] by strong energy confinement near the surface, low propagation loss, and high stability, which have led to their extensive applications in radio frequency,[2–4] signal processing,[5–7] and sensing.[8–10] The phonon modes in SAW resonators can be readily engineered to operate in the gigahertz frequency range, with quality factors reaching up to $\sim$ 100000 at cryogenic temperatures.[11,12] In recent years, with the rapid development of quantum technology, SAW has garnered significant attention in the field of quantum information processing, particularly in the SAW-qubit coupling.[13–15] Strong coherent coupling between SAW resonators and superconducting qubits has been experimentally demonstrated.[13,16–18] These interactions have enabled key quantum functionalities such as quantum state transfer,[14] multiphonon entanglement,[19] and realization of single-phonon beam splitters.[20]

Another promising avenue for the development of quantum computing involves semiconductor quantum dots (QDs), in which individual electrons are confined and manipulated to define qubits via their charge or spin degrees of freedom.[21] These nanostructures enable flexible qubit configurations. For example, in a double quantum dot (DQD), a charge qubit, a singlet–triplet qubit, or two coupled single-spin qubits can be encoded.[21] This platform offers several advantages, including scalability,[22] fast gate operations,[23] compatibility with existing semiconductor fabrication processes,[24] and potential for operation at elevated temperatures.[25–27]

SAW resonators offer excellent compatibility with semiconductor QDs, particularly due to their resilience to magnetic fields, which is a crucial requirement for most types of spin qubits.[21] In addition, the much lower speed of sound compared to light allows for more compact and easily controlled on-chip phononic structures. Previous studies have shown that the moving trapping potential of a traveling SAW can control and coherently transfer single electrons[28,29] and entangled electron spins[30] in quantum dots. However, despite these developments, studies on the coupling between SAW resonators and semiconductor DQDs, where charge and spin qubits are hosted, remain limited.

In this work, we propose a hybrid quantum architecture in which a SAW resonator is capacitively coupled to a semiconductor DQD. To mitigate losses, we adopt a flip-chip three-dimensional integration scheme, physically separating the piezoelectric SAW structure from the qubit layer. We consider practical factors such as the crystallographic cut of the lithium niobate (LN), SAW propagation direction, and transmission loss, and we estimate the coupling strength between a SAW phonon and a single electron trapped in the DQD using

[†]Corresponding author. E-mail: zzzhang@ustc.edu.cn

© 2026 Chinese Physical Society and IOP Publishing Ltd. All rights, including for text and data mining, AI training, and similar technologies, are reserved.

realistic device parameters. By comparing the estimated coupling strength with experimentally measured dissipation rates, we demonstrate that the system can enter the strong coupling regime, providing a scalable solid-state platform for investigating coherent phonon–electron interactions.

2. Design principle of the architecture

To build a functional hybrid quantum system, strong coupling between the constituent subsystems is essential. Specifically, the coupling strength must exceed the dissipation rates of both subsystems. In the case of coupling between phonons in a SAW resonator and electrons in a DQD, the primary mechanism involves a piezoelectric material. Here, mechanical deformation generates an associated electric potential that interacts with the electrons in the quantum dot.[31] It is worth noting that we neglect the deformation coupling, since its contribution is much smaller than that of the piezoelectric mechanism.[31,32]

Silicon is a particularly attractive host material for quantum dot qubits.[33] While it is technically possible to deposit a piezoelectric layer on silicon for electrical generation and detection of SAWs, doing so may introduce additional decoherence channels,[34] thereby compromising the performance of the nearby qubit. To boost coupling strength without degrading coherence, it is therefore crucial to optimize the transduction of mechanical vibrations into electric fields. In this work, we employ LN, a piezoelectric material with a high electromechanical coupling coefficient, as the substrate for the SAW resonator. To protect the silicon-based qubits from piezoelectric-induced decoherence, we implement a flip-chip architecture that physically separates the two systems: the SAW resonator is fabricated on an LN chip, while the DQD is hosted on a separate silicon chip.

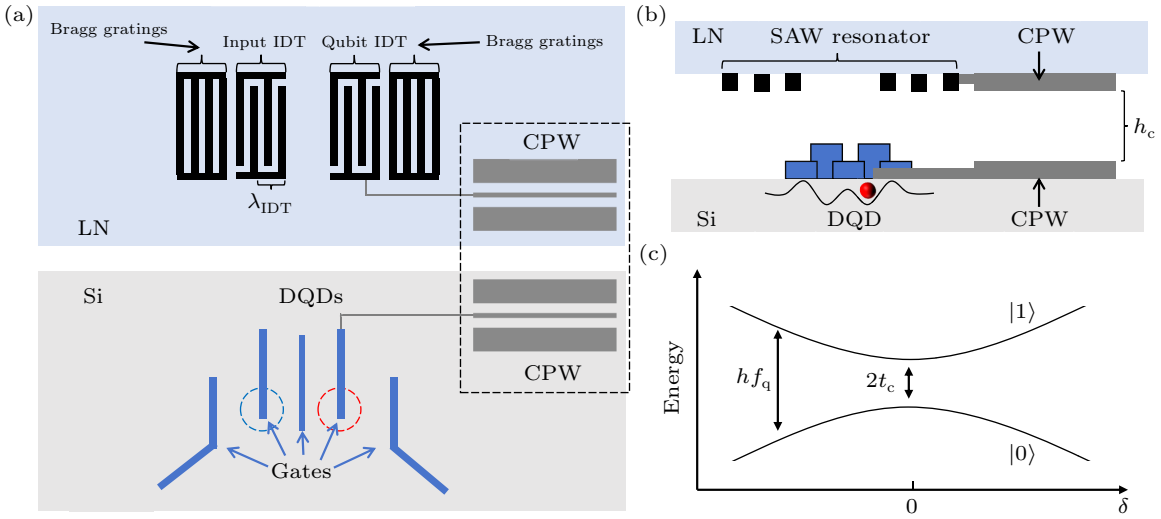


Fig. 1. Proposed 3D integration architecture. The structure consists of a SAW resonator on a lithium niobate (LN) substrate, double quantum dots (DQDs) on a silicon substrate, and two microwave coplanar waveguides (CPWs) on the two chips, respectively. (a) Plane schematic of the 3D integration architecture. The SAW resonator is composed of Bragg gratings and interdigital transducers (IDTs). The qubit IDT on the right side is connected to the central conductor of the CPW on LN. The DQD is capacitively linked to the CPW. (b) Cross-section schematic of the 3D integration architecture. The two CPWs form a flip-chip structure with a spacing of h_c. (c) Energy diagram of a semiconductor charge qubit hosted by a DQD.

As shown in the upper parts of Figs. 1(a) and 1(b), the SAW resonator consists of two interdigital transducers (IDTs) and two Bragg gratings. The frequency of the SAW resonator f_{SAW} is defined by the IDT electrode period λ_{IDT} and the speed of sound in the substrate v_{SAW}, with $f_{SAW} = v_{SAW}/\lambda_{IDT}$. One of the IDTs (labeled "qubit IDT") is connected to a microwave coplanar waveguide (CPW) for coupling. The two Bragg gratings act as acoustic mirrors, forming a Fabry–Pérot-like cavity for phonons. On the silicon chip shown in the lower parts of Figs. 1(a) and 1(b), the DQD is defined using patterned electrostatic gates, forming two closely spaced potential wells capable of confining a single electron beneath the gates. In this configuration, a charge qubit is encoded in the electron charge distribution within the two dots.[23] As shown in Fig. 1(c), the qubit transition frequency is $f_q = \sqrt{\delta^2 + 4t_c^2}/h$, where δ is the DQD energy-level detuning, t_c is the interdot tunnel coupling, and h is the Planck constant. A plunger gate of the DQD is connected to a separate CPW. The two chips are aligned and bonded (shown in Fig. 1(b)) such that the CPWs (with a spacing of h_c) on each chip form a coupling interface, enabling energy exchange between the SAW resonator and the DQD across the flip-chip structure. Compared to galvanic coupling, this structure is much easier to fabricate and offers substantially reduced inter-chip low-frequency noise transmission.[35–38]

Within this architecture, two key factors warrant further investigation. First, the crystallographic cut of the LN substrate and the propagation direction of the SAW significantly

influence its electromechanical coupling, thereby affecting the achievable SAW-DQD coupling strength. Second, the coupling geometry and misalignment between the CPWs during the flip-chip bonding process can lead to transmission loss, resulting in a weakened coupling strength in practical implementations. We examine these two factors as follows.

3. Effects of SAW propagation direction

The piezoelectricity can be described by the following equations:

$$\rho\ddot{u}_i - c_{ijkl}\partial_j\partial_l u_k = e_{kij}\partial_j\partial_k\Phi, \tag{1}$$

$$\varepsilon_{ij}\partial_i\partial_j\Phi = e_{ijk}\partial_i\partial_k u_j, \tag{2}$$

where summation is implied over repeated indices ($i, j, k, l = x, y, z$), $\boldsymbol{u}(\boldsymbol{x},t)$ is the displacement field ($\boldsymbol{x}$ is the Cartesian coordinate vector), ∂_i represents taking partial derivatives with respect to i, ρ is the density of the piezoelectric material; c_{ijkl}, e_{ijk}, and ε_{ij}, which depend on the crystallographic cut of the LN, are the elasticity tensor, piezoelectric tensor, and permittivity, respectively. Adopting free boundary conditions,[39] the propagation forms of SAW can be obtained. Through quantization, the mechanical displacement corresponding to each SAW phonon mode becomes an operator $\hat{\boldsymbol{u}}(x,t) = \sqrt{h/(2f_{\mathrm{SAW}})}(v\hat{b} + v^*\hat{b}^\dagger)$, where $\hat{b}$ and $\hat{b}^\dagger$ are the annihilation and creation operators of the phonon mode, respectively. v is the wave function of the phonon mode solved from Eqs. (1) and (2). By equating the classical energy of the SAW to the energy of a single phonon, we obtain the zero-point mechanical amplitude $\boldsymbol{U}_0$.[34] Substituting the obtained $\boldsymbol{U}_0$ into the known specific propagation form of the SAW yields the single-phonon piezoelectric potential ϕ_0,[31] which is analogous to the electric-field amplitude associated with a single photon in circuit quantum electrodynamics.[40] Here, we configure the SAW resonator to operate in the single-mode regime. In the multi-mode regime, ϕ_0 can be determined by computing the contribution of each individual mode and summing them, owing to the linearity of the piezoelectric equations and the mutual orthogonality of the phonon modes.

ϕ_0 is one of the core factors that determines the coupling strength and is strongly dependent on the propagation direction of the SAW, as LN is highly anisotropic. $1/\phi_0$ is also proportional to the square root of the effective area of the phonon mode, $\sqrt{S}$. Since S depends on the design of the resonator, in the subsequent calculation of the single-phonon piezoelectric potential, we evaluate $\phi_{\mathrm{LN}} = \phi_0 \times \sqrt{S}$ to normalize the contribution from S. ϕ_{LN} is the single-phonon piezoelectric potential at unit mode area. Rotating the propagation direction of the SAW around the crystal axes of the LN with a set of angles (A, B, C), the calculated ϕ_{LN} is presented in Fig. 2. Here, A, B, and C denote the rotation angles around the crystal axes Y, Z, and X, respectively.[41]

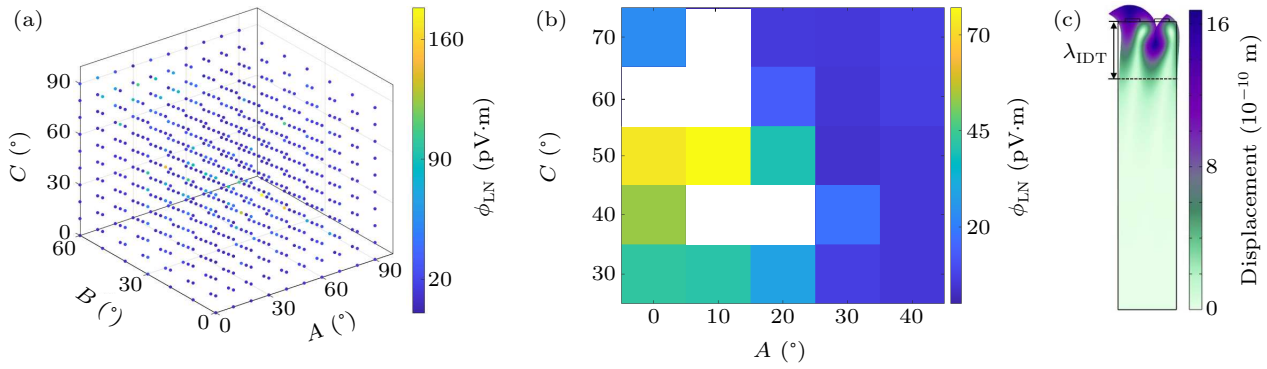


Fig. 2. Calculations of the piezoelectric potential associated with a single phonon. (a) Calculated ϕ_{LN} under different rotation-angle parameters (A, B, C), where A, B, and C denote the rotation angles of the SAW propagation direction around the crystal axes Y, Z, and X of the LN, respectively. (b) A slice extracted from (a) with $B = 30°$. Here, data points that are strongly influenced by non-surface waves in the SAW are masked in white. The angles near (10°, 30°, 50°) exhibit a high ϕ_{LN}. (c) The vibration mode simulated by COMSOL for an orientation corresponding to the rotation-angle set (15°, 30°, 53°). The black dashed line corresponds to a distance of λ_{IDT} from the surface.

Furthermore, at certain orientations, SAWs are significantly contaminated by non-surface modes, rendering the calculated ϕ_{LN} inaccurate. Therefore, for cuts with high ϕ_{LN}, we compare the theoretical sound velocities of SAWs with simulated results obtained using COMSOL. Cuts with significant discrepancies in sound velocity, where severe non-surface wave components are involved, are excluded. Thus, the selected cuts satisfy the following criteria: (i) high ϕ_{LN}, and (ii) minimal influence from non-surface waves on the SAW.

Along different directions on the surfaces of Y–Z and 128° Y–X LN, which are commonly used, ϕ_{LN} is found to be around 10 pV · m. As shown in Fig. 2(a), considering the symmetry of LN, we calculate ϕ_{LN} by varying A, B, and C within the ranges of 0° to 90°, 0° to 60°, and 0° to 90°, respectively, with an increment of 10°. It is found that near (10°, 30°, 50°), higher ϕ_{LN} values exist, with minimal influence from non-surface waves on the SAW. A slice on the plane of $B = 30°$ is shown in Fig. 2(b). By further reducing the scanning increment to 1°, the angle set (15°, 30°, 53°) is ultimately identified as the optimal rotation angle, at which ϕ_{LN} reaches

84.3 pV · m. Furthermore, we simulate the vibration mode corresponding to the angle set (15°, 30°, 53°), as shown in Fig. 2(c). The black dashed line corresponds to a distance of λ_{IDT} from the surface. It can be observed that the vibration is primarily confined within λ_{IDT} from the surface, indicating that it is predominantly attributed to surface modes rather than bulk modes. After optimization, the value of ϕ_{LN} is enhanced by a factor of 8 compared to that of the commonly used Y–Z and 128° Y–X LN.

4. Estimation of transmission loss in coupling CPWs

Transmission loss in the coupling CPWs is another practical factor that can affect the coupling strength. Figure 3(a) illustrates a top-view schematic of the flip-chip coupling structure within the central black dashed box in Fig. 1. The two CPWs form a capacitor-like structure. The key parameters of the structure include the width of the center conductor s, the coupling length l_{c}, the distance from the center conductor to the ground plane w, the width of the ground plane w_{ground}, and the spacing between the two chips h_{c}. To better reflect practical conditions, misalignments are considered. A deviation dy along the width direction of the center conductor occurs when the two CPW transmission lines are laterally misaligned. In addition, a non-zero angle $\Delta\mathrm{deg}\,y$ between the two lines arises when they are not parallel, as shown in Fig. 3(b). Figure 3(c) shows the schematic of two CPWs with unequal spacing, where $\Delta\mathrm{deg}\,z$ is the tilt angle.

Since the transmission is strongly dependent on the signal frequency, it is essential to fix the input frequency. The previously determined rotation angles (15°, 30°, 53°) correspond to a SAW velocity $v_{\mathrm{SAW}} = 3798$ m/s. We set the IDT electrode period λ_{IDT} to a practical value of 1 μm, yielding an input frequency equal to the resonant frequency of the SAW resonator, $f_{\mathrm{SAW}} = v_{\mathrm{SAW}}/\lambda_{\mathrm{IDT}} = 3.798$ GHz. This frequency also enables resonant coupling with the DQD charge qubit, offering a larger effective coupling strength.[42] We construct a model based on our design in COMSOL and simulate the S_{21} parameter between two ports on individual chips to quantify the transmission loss, as illustrated in Fig. 3(d).

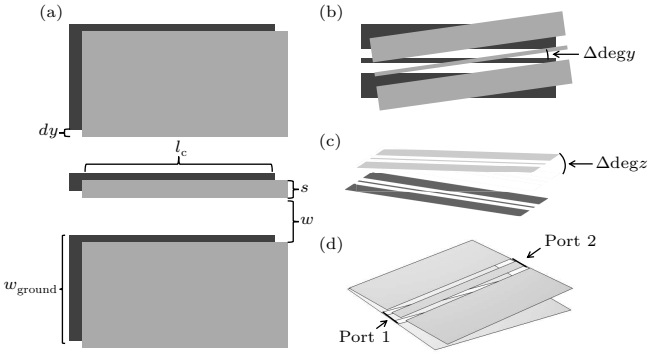


Fig. 3. Schematic of the flip-chip coupling CPWs. (a) A top-view schematic of the flip-chip coupling structure. Here, s is the width of the center conductor, l_{c} is the coupling length, w is the distance from the center conductor to the ground plane, w_{ground} is the width of the ground plane, and the spacing between the two CPW lines is h_{c} (shown in Fig. 1). dy is the deviation induced by misalignment. (b) Schematic of two non-parallel CPWs, with a non-zero angle $\Delta\mathrm{deg}\,y$ between them. (c) Schematic of two CPWs with unequal spacing, where $\Delta\mathrm{deg}\,z$ is the tilt angle. (d) Schematic of the flip-chip coupling structure in COMSOL. Port 1 and port 2 are the input and output ports, respectively.

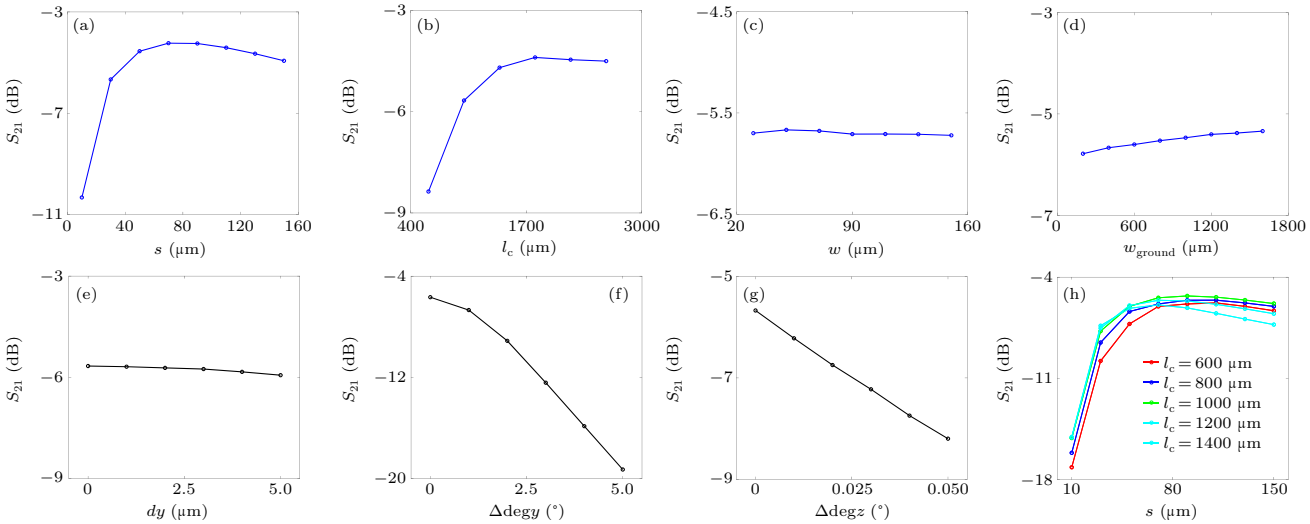


Fig. 4. Influence of the main geometric parameters of the coupling structure on S_{21}. (a)–(d) Influence of s, l_{c}, w, and w_{ground} on S_{21}, respectively. When one parameter is scanned, all other parameters are fixed. (e)–(g) Influence of dy, $\Delta\mathrm{deg}\,y$, and $\Delta\mathrm{deg}\,z$ induced by misalignment on S_{21}, respectively. (h) Based on the preceding results and experimental considerations, influence of s on S_{21} with $l_{\mathrm{c}} = 600$ μm, 800 μm, 1000 μm, 1200 μm, and 1400 μm, respectively.

According to relevant studies,[35] smaller h_{c} values lead to higher S_{21}. However, practical limitations prevent h_{c} from being reduced indefinitely. In this study, we first set h_{c} to an achievable low value[35] of 1 μm. We then simulate the dependence of S_{21} on each of the parameters s, l_{c}, w, and w_{ground}, while maintaining all others fixed, as shown in Figs. 4(a)–4(d),

respectively. When fixed, s, l_c, w, and w_{ground} are set to 30 μm, 1000 μm, 50 μm, and 400 μm, respectively. These values are all based on achievable experimental conditions. From Figs. 4(a)–4(b), it can be observed that as l_c or s increases individually, S_{21} first increases and then remains nearly constant within a practical range. Although significant changes are applied to w or w_{ground}, the variation in S_{21} remains within ±0.5 dB, indicating that both w and w_{ground} have a negligible influence on S_{21}, as shown in Figs. 4(c)–4(d).

Next, we investigate the influence of possible misalignment in the flip-chip assembly, with $s = 30$ μm, $w = 50$ μm, $l_c = 1000$ μm, and $w_{ground} = 400$ μm. Figure 4(e) illustrates the dependence of S_{21} on dy. Increasing dy from 0 to 5 μm results in a reduction of approximately 0.4 dB in S_{21}, indicating a minor influence. As shown in Fig. 4(f), when $\Delta\deg y$ increases from 0° to 5°, S_{21} decreases by approximately 14 dB. Figure 4(g) illustrates the influence of $\Delta\deg z$ on S_{21}. The variation in S_{21} induced by $\Delta\deg z$ is about 4 dB when $\Delta\deg z$ increases from 0° to 0.05°.

Within the investigated parameter space, the effect of dy can be ignored. In further investigation, $\Delta\deg y$ is set to 1°, and $\Delta\deg z$ is set to 0.02°. We then revisit the choice of l_c and s. As shown in Fig. 4(h), when $l_c = 1000$ μm and $s = 90$ μm, S_{21} reaches its maximum value of approximately −5.3 dB. It can be found that within the investigated range, S_{21} varies over a span of ∼ 12 dB, which could severely degrade the coupling strength.

5. Result and discussion

After optimizing the factors discussed above, we evaluate the coupling strength. Considering that the piezoelectric potential guided by the CPW directly interacts with the charge qubit in the DQD, we describe the hybrid system using the following Jaynes–Cummings–type Hamiltonian:[43]

$$H = \frac{hf_q}{2}\sigma^z + hf_{SAW}a^\dagger a + \frac{hg_c}{2\pi}\left(\sigma^+ a + \sigma^- a^\dagger\right), \tag{3}$$

where σ^+ and $a^\dagger$ are the creation operators of the qubit and phonon, respectively, while σ^- and a are the corresponding annihilation operators. The effective resonant coupling strength g_c is defined as[31]

$$g_c = \frac{2\pi e\phi_0 G}{h}\cdot\frac{2t_c}{hf_q}. \tag{4}$$

Here, $G = S_{21}\alpha$ is associated with the geometric parameters of the coupling structure, and α is the lever arm of the coupling electrode on the DQD. Considering practical experimental conditions and setting the IDT electrode period to 1 μm, the effective mode area is $S = 125$ μm^2. According to our previous calculations, ϕ_{LN} corresponding to rotation angles (15°, 30°, 53°) reaches an optimal value of 84.3 pV · m. Therefore, $\phi_0 = \phi_{LN}/\sqrt{S} = 7.5$ μV. The S_{21} of the coupling CPWs is set to −5.3 dB, corresponding to a factor of 0.54.

Considering a charge qubit operating at its sweet spot with DQD energy-level detuning $\delta = 0$, we have $hf_q = 2t_c$. Meanwhile, the lever arm α can reach values as high as 0.35.[44] If the SAW substrate is Y–Z or 128° Y–X LN, g_c lies in the range of $40\times2\pi$–$50\times2\pi$ MHz. With the optimized orientation, g_c can be significantly enhanced to $346.7\times2\pi$ MHz. The practical decoherence rate γ of charge qubits is on the order of $10\times2\pi$–$60\times2\pi$ MHz,[45–47] while the dissipation rate of the SAW resonator can be optimized to $\kappa = 0.1$–1 MHz. Since g_c exceeds both γ and κ, the system enters the strong-coupling regime.

From the above analysis, we conclude that the SAW propagation direction and the coupling-geometry settings must be carefully engineered in future experiments to realize enhanced coupling strength. Due to its evanescent nature, the piezoelectric potential in vacuum decays exponentially with distance from the surface. At a height of one wavelength, comparable to the separation between the two substrates in our design, the piezoelectric potential attenuates to approximately 1/1000 of its surface value. However, additional pathways may exist through which the piezoelectric potential can propagate to the DQD, such as capacitances between the IDTs and DQD electrodes. These "leaked" piezoelectric potentials can interact with the charge qubit via a Hamiltonian of the same form as Eq. (4), potentially leading to higher coupling strengths in realistic situations.

By engineering the electron spin–orbit coupling within the DQD, it is also possible to realize coherent spin–phonon coupling,[45,48] thereby extending the versatility of this hybrid architecture. It is worth noting that our design is not limited to silicon-based devices.[33,49–52] Since the two substrates are physically separated, this approach is also applicable to other material platforms such as GaAs,[23,53,54] graphene,[55–60] and MoS_2.[56,61,62] For example, the exceptional electronic and mechanical properties of graphene [63–65] offer the possibility of coupling SAW phonons to electrons' charge, spin, and valley degrees of freedom.[66–69]

6. Conclusion

In this study, we propose a three-dimensional integration architecture that combines a SAW resonator with a semiconductor DQD. By optimizing the SAW propagation direction and the geometric parameters of the flip-chip coupling structure, we have estimated the coupling strength between the SAW resonator and the DQD to be $346.7\times2\pi$ MHz, reaching the strong coupling regime. The theoretical framework and design principles established here lay the groundwork for the experimental realization of strong coupling between SAW

phonons and electrons in DQD. This architecture further provides a promising route toward long-range coupling between semiconductor charge and spin qubits mediated by phonons in SAW resonators.

Acknowledgments

This project was supported by the National Natural Science Foundation of China (Grant Nos. 12274401, 12274397, and 12034018), the National Key Research and Development Program of China (Grant No. 2022YFA1405900), and the Natural Science Foundation of Jiangsu Province (Grant No. BK20240123).

References

[1] Morgan D 2007 *Surface Acoustic Wave Filters: With Applications to Electronic Communications and Signal Processing* (Oxford: Elsevier Science)
[2] Bell D L T and Li R C M 1976 *Proc. IEEE* **64** 711
[3] Shao L, Zhu D, Colangelo M, Lee D, Sinclair N, Hu Y, Rakich P T, Lai K, Berggren K K and Lončar M 2022 *Nat. Electron.* **5** 348
[4] Hackett L, Miller M, Brimigion F, Dominguez D, Peake G, Tauke-Pedretti A, Arterburn S, Friedmann T A and Eichenfield M 2021 *Nat. Commun.* **12** 2769
[5] Maines J D and Paige E G S 1976 *Proc. IEEE* **64** 639
[6] Mayor F M, Jiang W, Sarabalis C J, McKenna T P, Witmer J D and Safavi-Naeini A H 2021 *Phys. Rev. Appl.* **15** 014039
[7] Hackett L, Miller M, Weatherred S, Arterburn S, Storey M J, Peake G, Dominguez D, Finnegan P S, Friedmann T A and Eichenfield M 2023 *Nat. Electron.* **6** 76
[8] Li B, Lin Q and Li M 2023 *Nature* **620** 316
[9] Kim Y, Suh J M, Shin J, Liu Y, Yeon H, Qiao K, Kum H S, Kim C, Lee H E, Choi C, Kim H, Lee D, Lee J, Kang J H, Park B I, Kang S, Kim J, Kim S, Perozek J A, Wang K, Park Y, Kishen K, Kong L, Palacios T, Park J, Park M C, Kim H J, Lee Y S, Lee K, Bae S H, Kong W, Han J and Kim J 2022 *Science* **377** 859
[10] Okuda S, Ono T, Kanai Y, Ikuta T, Shimatani M, Ogawa S, Maehashi K, Inoue K and Matsumoto K 2018 *ACS Sens.* **3** 200
[11] Manenti R, Peterer M J, Nersisyan A, Magnusson E B, Patterson A and Leek P J 2016 *Phys. Rev. B* **93** 041411
[12] Emser A L, Rose B C, Sletten L R, Aramburu Sanchez P and Lehnert K W 2022 *Appl. Phys. Lett.* **121** 224001
[13] Andersson G, Suri B, Guo L, Aref T and Delsing P 2019 *Nat. Phys.* **15** 1123
[14] Bienfait A, Satzinger K J, Zhong Y P, Chang H S, Chou M H, Conner C R, Dumur É, Grebel J, Peairs G A, Povey R G and Cleland A N 2019 *Science* **364** 368
[15] Maity S, Shao L, Bogdanović S, Meesala S, Sohn Y I, Sinclair N, Pingault B, Chalupnik M, Chia C, Zheng L, Lai K and Lončar M 2020 *Nat. Commun.* **11** 193
[16] Bolgar A N, Zotova J I, Kirichenko D D, Besedin I S, Semenov A V, Shaikhaidarov R S and Astafiev O V 2018 *Phys. Rev. Lett.* **120** 223603
[17] Ruan X H, Li L, Liang G H, Zhao S L, Wang J H, Bu Y Z, Chen B J, Song X H, Li X, Zhang H, Wang J Z, Zhao Q C, Xu K, Fan H, Liu Y X, Zhang J, Peng Z H, Xiang Z C and Zheng D N 2024 *Appl. Phys. Lett.* **125** 052603
[18] Chen J F, He X L, Gao W P, Liu X Y, Niu Z Q, Liu K, Peng W, Wang Z and Lin Z R 2025 *Appl. Phys. Lett.* **126** 144001
[19] Andersson G, Jolin S W, Scigliuzzo M, Borgani R, Tholén M O, Rivera Hernández J C, Shumeiko V, Haviland D B and Delsing P 2022 *PRX Quantum* **3** 010312
[20] Qiao H, Dumur É, Andersson G, Yan H, Chou M H, Grebel J, Conner C R, Joshi Y J, Miller J M, Povey R G, Wu X and Cleland A N 2023 *Science* **380** 1030
[21] Burkard G, Ladd T D, Pan A, Nichol J M and Petta J R 2023 *Rev. Mod. Phys.* **95** 025003
[22] Zajac D M, Hazard T M, Mi X, Nielsen E and Petta J R 2016 *Phys. Rev. Appl.* **6** 054013
[23] Cao G, Li H O, Tu T, Wang L, Zhou C, Xiao M, Guo G C, Jiang H W and Guo G P 2013 *Nat. Commun.* **4** 1401
[24] Neyens S, Zietz O K, Watson T F, Luthi F, Nethwewala A, George H C, Henry E, Islam M, Wagner A J, Borjans F, Connors E J, Corrigan J, Curry M J, Keith D, Kotlyar R, Lampert L F, Małdzik M T, Millard K, Mohiyaddin F A, Pellerano S, Pillarisetty R, Ramsey M, Savytskyy R, Schaal S, Zheng G, Ziegler J, Bishop N C, Bojarski S, Roberts J and Clarke J S 2024 *Nature* **629** 80
[25] Han Lim W, Tanttu T, Youn T, Huang J Y, Serrano S, Dickie A, Yianni S, Hudson F E, Escott C C, Yang C H, Laucht A, Saraiva A, Chan K W, Cifuentes J D and Dzurak A S 2025 *Nano Lett.* **25** 10263
[26] Huang J Y, Su R Y, Lim W H, Feng M, van Straaten B, Severin B, Gilbert W, Dumoulin Stuyck N, Tanttu T, Serrano S, Cifuentes J D, Hansen I, Seedhouse A E, Vahapoglu E, Leon R C C, Abrosimov N V, Pohl H J, Thewalt M L W, Hudson F E, Escott C C, Ares N, Bartlett S D, Morello A, Saraiva A, Laucht A, Dzurak A S and Yang C H 2024 *Nature* **627** 772
[27] Camenzind L C, Geyer S, Fuhrer A, Warburton R J, Zumbühl D M and Kuhlmann A V 2022 *Nat. Electron.* **5** 178
[28] Hermelin S, Takada S, Yamamoto M, Tarucha S, Wieck A D, Saminadayar L, Bäuerle C and Meunier T 2011 *Nature* **477** 435
[29] McNeil R P G, Kataoka M, Ford C J B, Barnes C H W, Anderson D, Jones G A C, Farrer I and Ritchie D A 2011 *Nature* **477** 439
[30] Jadot B, Mortemousque P A, Chanrion E, Thiney V, Ludwig A, Wieck A D, Urdampilleta M, Bäuerle C and Meunier T 2021 *Nat. Nanotechnol.* **16** 570
[31] Schuetz M J A, Kessler E M, Giedke G, Vandersypen L M K, Lukin M D and Cirac J I 2015 *Phys. Rev. X* **5** 031031
[32] Naber W J M, Fujisawa T, Liu H W and van der Wiel W G 2006 *Phys. Rev. Lett.* **96** 136807
[33] Zwanenburg F A, Dzurak A S, Morello A, Simmons M Y, Hollenberg L C L, Klimeck G, Rogge S, Coppersmith S N and Eriksson M A 2013 *Rev. Mod. Phys.* **85** 961
[34] Kornich V, Kloeffel C and Loss D 2014 *Phys. Rev. B* **89** 085410
[35] Satzinger K J, Conner C R, Bienfait A, Chang H S, Chou M H, Cleland A Y, Dumur É, Grebel J, Peairs G A, Povey R G, Whiteley S J, Zhong Y P, Awschalom D D, Schuster D I and Cleland A N 2019 *Appl. Phys. Lett.* **114** 173501
[36] Gao J, Shen L, Li H, Ye S, Li J, Xu X, Cui J, Gao Y, Huang R and Ye L 2023 *IEEE International Solid-State Circuits Conference (ISSCC)*, Feb. 19–23, 2023, San Francisco, United States of America, pp. 346–348
[37] Rosenberg D, Kim D, Das R, Yost D, Gustavsson S, Hover D, Krantz P, Melville A, Racz L, Samach G O, Weber S J, Yan F, Yoder J L, Kerman A J and Oliver W D 2017 *npj Quantum Inf.* **3** 42
[38] Foxen B, Mutus J Y, Lucero E, Graff R, Megrant A, Chen Y, Quintana C, Burkett B, Kelly J, Jeffrey E, Yang Y, Yu A, Arya K, Barends R, Chen Z, Chiaro B, Dunsworth A, Fowler A, Gidney C, Giustina M, Huang T, Klimov P, Neeley M, Neill C, Roushan P, Sank D, Vainsencher A, Wenner J, White T C and Martinis J M 2018 *Quantum Sci. Technol.* **3** 014005
[39] Simon S H 1996 *Phys. Rev. B* **54** 13878
[40] Blais A, Grimsmo A L, Girvin S M and Wallraff A 2021 *Rev. Mod. Phys.* **93** 025005
[41] Gopalan V, Dierolf V and Scrymgeour D A 2007 *Annu. Rev. Mater. Res.* **37** 449
[42] Mi X, Cady J V, Zajac D M, Deelman P W and Petta J R 2017 *Science* **355** 156
[43] Childress L, Sørensen A S and Lukin M D 2004 *Phys. Rev. A* **69** 042302
[44] Zhang X, Hu R Z, Li H O, Jing F M, Zhou Y, Ma R L, Ni M, Luo G, Cao G, Wang G L, Hu X, Jiang H W, Guo G C and Guo G P 2020 *Phys. Rev. Lett.* **124** 257701
[45] Samkharadze N, Zheng G, Kalhor N, Brousse D, Sammak A, Mendes U C, Blais A, Scappucci G and Vandersypen L M K 2018 *Science* **359** 1123
[46] Yu C X, Zihlmann S, Abadillo-Uriel J C, Michal V P, Rambal N, Niebojewski H, Bedecarrats T, Vinet M, Dumur É, Filippone M, Bertrand B, De Franceschi S, Niquet Y M and Maurand R 2023 *Nat. Nanotechnol.* **18** 741
[47] Mi X, Benito M, Putz S, Zajac D M, Taylor J M, Burkard G and Petta J R 2018 *Nature* **555** 599
[48] Borjans F, Croot X G, Mi X, Gullans M J and Petta J R 2020 *Nature* **577** 195

[49] Wang K, Xu G, Gao F, Liu H, Ma R L, Zhang X, Wang Z N, Cao G, Wang T, Zhang J J, Culcer D, Hu X D, Jiang H W, Li H O, Guo G C and Guo G P 2022 *Nat. Commun.* **13** 206

[50] Wang N, Kang J M, Lu W L, Wang S M, Wang Y J, Li H O, Cao G, Wang B C and Guo G P 2024 *Nano Lett.* **24** 13126

[51] Zhang Z Z, Hu Q T, Song X X, Ying Y, Li H O, Zhang Z and Guo G P 2020 *Adv. Mater.* **32** 2005625

[52] Chu N, Zhu S K, Li A R, Wang C, Liao W Z, Cao G, Li H O and Guo G P 2025 *Chin. Phys. B* **34** 040303

[53] Gu S S, Kohler S, Xu Y Q, Wu R, Jiang S L, Ye S K, Lin T, Wang B C, Li H O, Cao G and Guo G P 2023 *Phys. Rev. Lett.* **130** 233602

[54] Lin T, Gu S S, Xu Y Q, Jiang S L, Ye S K, Wang B C, Li H O, Guo G C, Zou C L, Hu X D, Cao G and Guo G P 2023 *Nano Lett.* **23** 4176

[55] Qin G Q, Jing F M, Hao T Y, Jiang S L, Zhang Z Z, Cao G, Song X X and Guo G P 2025 *Phys. Rev. Lett.* **134** 036301

[56] Jing F M, Zhang Z Z, Qin G Q, Luo G, Cao G, Li H O, Song X X and Guo G P 2022 *Adv. Quantum Technol.* **5** 2100162

[57] Jing F M, Qin G Q, Zhang Z Z, Song X X and Guo G P 2023 *Appl. Phys. Lett.* **123** 184001

[58] Jing F M, Shen Z X, Qin G Q, Zhang W K, Lin T, Cai R, Zhang Z Z, Cao G, He L X, Song X X and Guo G P 2025 *Phys. Rev. Appl.* **23** 044053

[59] Banszerus L, Möller S, Hecker K, Icking E, Watanabe K, Taniguchi T, Hassler F, Volk C and Stampfer C 2023 *Nature* **618** 51

[60] Denisov A O, Reckova V, Cances S, Ruckriegel M J, Masseroni M, Adam C, Tong C, Gerber J D, Huang W W, Watanabe K, Taniguchi T, Ihn T, Ensslin K and Duprez H 2025 *Nat. Nanotechnol.* **20** 494

[61] Zhang Z Z, Song X X, Luo G, Deng G W, Mosallanejad V, Taniguchi T, Watanabe K, Li H O, Cao G, Guo G C, Nori F and Guo G P 2017 *Sci. Adv.* **3** e1701699

[62] Kumar P, Kim H, Tripathy S, Watanabe K, Taniguchi T, Novoselov K S and Kotekar-Patil D 2023 *Nanoscale* **15** 18203

[63] Wang Y B, Zhang Z Z, Wu C X, Zhang Y S, Lei G S, Song X X and Guo G P 2025 *Chin. Phys. Lett.* **42** 070803

[64] Novoselov K S, Geim A K, Morozov S V, Jiang D, Katsnelson M I, Grigorieva I V, Dubonos S V and Firsov A A 2005 *Nature* **438** 197

[65] Blees M K, Barnard A W, Rose P A, Roberts S P, McGill K L, Huang P Y, Ruyack A R, Kevek J W, Kobrin B, Muller D A and McEuen P L 2015 *Nature* **524** 204

[66] Fang Y, Xu Y, Kang K, Davaji B, Watanabe K, Taniguchi T, Lal A, Mak K F, Shan J and Ramshaw B J 2023 *Phys. Rev. Lett.* **130** 246201

[67] Mou Y C, Wang J Y, Chen H N, Xia Y C, Li H L, Yan Q, Jiang X, Wu Y J, Shi W, Jiang H, Xie X C and Zhang C 2025 *Phys. Rev. Lett.* **134** 096301

[68] Cao X Y, Jia Z H, Mou Y C, Zhang S H, Yang J S, Zhang Y D, Dai W J, Gu J M, Chen H N, Qian L, Jiang C, Xie X Y, Zhou Z Q, Yan J Y, Jiang H, Watanabe K, Taniguchi T, Dong S M, Xie X C, Zhang C and Xiu F X 2025 *Nano Lett.* **25** 9535

[69] Qin G Q, Wang Y B, Lei G S, Zhang Z Z, Song X X and Guo G P 2025 *Chin. Phys. B* **34** 018801